Published in final edited form as:

Cancer Cell. 2015 October 12; 28(4): 415–428. doi:10.1016/j.ccell.2015.09.004.

Structural design of engineered costimulation determines tumor rejection kinetics and persistence of CAR T cells

Zeguo Zhao[1,*], **Maud Condomines**[1,*], **Sjoukje J.C. van der Stegen**[1], **Fabiana Perna**[1], **Christopher C. Kloss**[1], **Gertrude Gunset**[1], **Jason Plotkin**[1], and **Michel Sadelain**[1,2,#]

[1]Center for Cell Engineering, Memorial Sloan Kettering Cancer Center, New York, NY, 10065, USA

[2]Immunology Program, Sloan Kettering Institute, New York, NY, 10065, USA

Summary

T cell engineering is a powerful means to rapidly generate anti-tumor T cells. The costimulatory properties of second-generation chimeric antigen receptors (CARs) determine the overall potency of adoptively transferred T cells. Utilizing an in vivo “stress test” to challenge CD19-targeted T cells, we studied the functionality and persistence imparted by 7 different CAR structures providing CD28 and/or 4-1BB costimulation. One configuration, which utilizes two signaling domains (CD28 and CD3ζ) and the 4-1BB ligand, provided the highest therapeutic efficacy, showing balanced tumoricidal function and increased T cell persistence accompanied by an elevated CD8/CD4 ratio and decreased exhaustion. Remarkably, induction of the IRF7/IFNβ pathway was required for optimal anti-tumor activity. Thus, 1928z-41BBL T cells possess strikingly potent intrinsic and immunomodulatory qualities.

Graphical abstract

[#]To whom correspondence should be addressed. m-sadelain@ski.mskcc.org.
[*]These authors contributed equally to this work.

Authorship Contributions

Z.Z. and M.C. designed the study, designed and performed experiments, analyzed and interpreted data, and wrote the manuscript; S.J.C.vdS. designed and performed experiments, analyzed and interpreted data, and wrote the manuscript; F.P. contributed to microarray analyses; C.C.K. performed experiments; J.P. and G.G. contributed to vector construction, T cell transduction and animal studies; M.S. designed the study, analyzed and interpreted data, and wrote the manuscript.

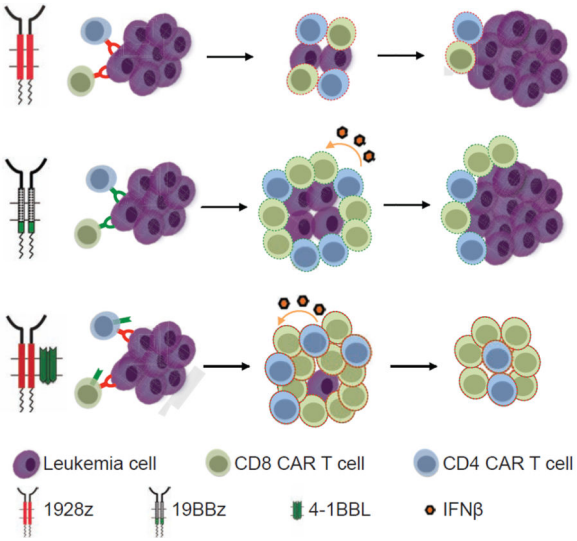

Introduction

T cell engineering allows for rapid generation of T cells of any desired specificity. The rationale for this approach to cancer immunotherapy is to bypass the barriers to active immunization in order to establish T cell-mediated tumor immunity (Brentjens et al., 2003; Ho et al., 2003). Chimeric antigen receptors (CARs) are recombinant receptors for antigen, which, in a single molecule, redirect T cell specificity and eventually enhance anti-tumor potency. Functional augmentation is achieved through the design of second generation CARs, which not only redirect cytotoxicity, but also reprogram T cell function and longevity through their costimulatory properties (Sadelain et al., 2009; van der Stegen et al., 2015). Thus, human peripheral blood T cells that engage antigen through a second generation CAR receive both activating and costimulatory signals, resulting in cytotoxity as well as proliferation in the presence of tumor antigen, irrespective of the presence of costimulatory ligands (Maher et al., 2002). T cells that stably express second generation CARs thus acquire supra-physiological properties and become “living drugs” that exert both immediate and long-term therapeutic effects (Sadelain et al., 2009).

Two decades ago, we selected CD19 as the prime target for developing our CAR technology (Sadelain, 2015). Using immunodeficient mice bearing a broad range of B cell malignancies, including acute lymphoblastic leukemia (ALL), we showed a single intravenous infusion of CD19 CAR targeted T cells could eradicate tumor and induce long-term remissions (Brentjens et al., 2003). CD19 has since become the poster child for CAR therapies. Two types of second generation CARs, utilizing either CD28 (Maher et al., 2002) or 4-1BB (Imai et al., 2004) as signaling components, have been used in patients, both have yielded dramatic outcomes. Complete remissions have been obtained in patients with various B cell malignancies, most consistently in ALL (Brentjens et al., 2011; Davila et al., 2014; Grupp et al., 2013; Lee et al., 2015; Maude et al., 2014), reviewed in (Davila et al., 2012; Ramos et al., 2014).

We model CD19 CAR therapy of ALL to evaluate CAR designs that differ in their structural recruitment of CD28 and 4-1BB signaling with the aim to unravel the subtlety of providing optimal costimulatory support to engineered T cells.

Results

CD28 and 4-1BB costimulation induce different tumor elimination kinetics

To compare the impact of the CD28 and 4-1BB costimulatory domains of CARs on T cell anti-tumor functionality, we first assessed the proliferative and cytolytic potential of 1928z and 19BBz T cells, utilizing a first generation CAR (19z1) as reference (Figure S1A). To exclude potentially confounding effects imparted by different levels of CAR expression, we conducted all studies using the same vector design (constant enhancer/promoter and bicistronic vector structure) and strived to achieve comparable CAR expression levels in all T cell groups within each experiment (Figures 1A, S1B and S1C). In vitro, the 19z1, 1928z and 19BBz T cell groups showed near-identical cytolytic capacity (Figure 1B). However, in proliferation assays (without addition of exogenous cytokines), both second generation CARs showed greater T cell expansion and accumulation upon weekly antigen stimulation, with the 19BBz CAR outperforming 1928z after two or three weeks (Figure 1C). To further compare the therapeutic potential of peripheral blood T cells transduced with these CARs, we devised a T cell “stress test” in which T cell doses are purposefully lowered to levels where CAR therapy begins to fail, based on the previously described NALM/6 pre-B ALL model (Brentjens et al., 2003; Brentjens et al., 2007). Here, we lowered the treatment dose to 4×10^5, 2×10^5 and 1×10^5 CAR T cells (Figure 1D). Efficacy of tumor eradication decreased with dose reduction within all groups, with both second generation CARs consistently performing better than the first generation construct (Figures 1D and 1E). The 1928z CAR consistently showed more rapid tumor elimination and could still induce a few complete remissions at a dose of 4×10^5 T cells, but no longer at lower doses (Figures 1D and 1E). However, survival was still significantly extended at a dose of 2×10^5 CAR T cells (Figure 1E). The 19BBz CAR also delayed tumor progression, albeit with noticeably slower kinetics than 1928z, as increasingly obvious at lower T cell doses (2×10^5 and 1×10^5) (Figure 1D). To further analyze the kinetic differences in tumor control between the different CARs, CAR T cells and tumor cells were enumerated 7, 14 and 21 days post-infusion in the bone marrow (Figures 2A and S2A) and spleen (Figure S2B) in animals treated at the suboptimal T cell dose of 2×10^5 CAR T cells. At day 7, CAR T cells accumulated to the same level for both second generation constructs, but 1928z T cells had already eliminated more tumor cells than 19BBz (Figure 2A), confirming the more rapid tumor elimination detected by bioluminescence (Figure 1D). By day 14 and 21, 19BBz T cells surpassed 1928z T cells in number and gradually caught up to 1928z T cells in terms of tumor cell elimination (Figure 2A). In contrast, the first generation 19z1 construct induced only modest T cell accumulation, insufficient to achieve tumor control despite evident tumor elimination at early time points (Figure 2A). Examination of T cell and tumor cell numbers at multiple time points further reinforces the differential kinetics of these different CARs (Figure 2B). Only 1928z T cells were able to induce a substantial tumor reduction during the first seven days. Owing to limited expansion, 19z1 T cells maintained a low effector:target (E:T) ratio and failed to achieve tumor control (Figures 2B and 2C). Although 19BBz T cells

accumulated to higher levels than 1928z T cells by day 14, comparable tumor cell elimination was still not achieved. (Figure 2B). These measurements reveal that tumor eradication by 1928z T cells is superior to 19BBz T cells, because tumor cell elimination is achieved with a lower in vivo E:T ratio (Figure 2C). In aggregate, these analyses confirm the enhanced expansion and function of second generation CARs but further reveal the greater functional potential of 1928z T cells, which is compensated but not exceeded over time by 19BBz T cells, owing to their greater persistence.

Balancing effector and persistence functions through optimally combined costimulation

Recognizing the distinct kinetic functions of the CD28 and 4-1BB-based CARs, we hypothesized that an optimal combination of these two costimulatory signals would result in both accelerated and more profound tumor eradication if the properties of each CAR could be cumulated and reconciled. We therefore designed four configurations whereby the CD3ζ-mediated activation and both CD28 and 4-1BB signals are solicited. The 1928BBz CAR is a third generation CAR design, as previously described (Zhong et al., 2010). 19z1-CD80-41BBL utilizes two costimulatory ligands, as previously described in (Stephan et al., 2007) (Figure S3A). The 1928z-41BBL, and 19BBz-CD80 configurations combine each second generation CAR with the “complementary” costimulatory ligand (Figure S3A). As in the above studies (Figures 1 and 2), comparable levels of CAR expression were achieved, except for 1928BBz (Figure 3A). This CAR was consistently expressed at a lower level (Figures S3B and S3C), consistent with most other studies making use of triple-signaling CARs (Carpenito et al., 2009; Tammana et al., 2010; Zhao et al., 2009). All constructs had similar cytolytic capacity in vitro (Figure 3B), which did not differ from their first and second generation counterparts (Figure 1B). Expansion upon weekly antigen stimulation without exogenous cytokines was enhanced for all constructs compared to the second generation CARs, except for the 1928BBz construct, and strongest for the 1928z-41BBL configuration (Figure 3C). In vivo, however, the constructs yielded very different outcomes. Among the three superior combinations, 1928z-41BBL consistently emerged as the most potent, as reflected in most effective tumor eradication, highest frequency of long-term complete remission and highest survival rates at the low dose of 1×10^5 CAR T cells (Figures 3D and 3E). The enumeration of CAR T cells and tumor cells in the bone marrow (Figures 4A and S4A) and spleen (Figure S4B) showed that 1928z-41BBL T cells displayed the most elevated, early T cell accumulation and most profound tumor cell eradication. Interestingly, despite poor T cell accumulation during the first week, 1928BBz T cells induced significant early tumor control. However, these T cells failed to expand and induce complete tumor eradication. Both 19BBz-CD80 and 19z1-CD80-41BBL accumulated to similar levels as 1928z-41BBL by two weeks after T cell injection, however tumor cell elimination was less than with the latter. The 19z1-CD80-41BBL T cells eventually accumulated to high counts but were not able to prevent tumor progression (Figures 4A and 4B). Measuring the T cell and tumor cell counts within the different groups over time clearly shows that the strongest initial T cell expansion is achieved with 1928z-41BBL, resulting in rapid tumor cell clearance within the first seven days, more prolonged T cell persistence, eventually followed by T cell contraction. The delayed expansion and weaker effector function of 19BBz-CD80 and 19z1-CD80-41BBL allows for tumor cell expansion resulting in lower E:T ratios at early time points which may eventually reach tumor eradication levels over time (Figures 4B

and 4C). We verified that cytotoxic functions were maintained in vivo by performing ex vivo cytotoxicity assays using cells retrieved from the spleen 3 weeks after injection. All three combinatorial designs showed effective cytolytic function (Figure 4D), similar to preinfusion levels (Figure 3B), albeit slightly higher for the 1928z-41BBL T cells (Figure 4D).

Impact on CD4 and CD8 T cell persistence

We further analyzed the phenotype of the persisting CD4 and CD8 T cells, focusing on the their relative ratio, phenotype and expression of costimulatory receptors and exhaustion markers. The absolute cell counts of CD4 and CD8 T cell accumulation at the tumor site (bone marrow) and in the spleen are shown in Figures S2A, S2B, S4A and S4B. Two major patterns of CD8/CD4 ratio were observed. In most groups, the ratio remained stable over 3 weeks, similar to the infusion ratio (Figure 5A). Two of the groups, corresponding to the two groups expressing 4-1BBL, however diverged, showing a inversion of the CD8/CD4 ratio: 1928z-41BBL and 19z1-CD80-41BBL (Figures S5A and 5A). The 19BBz group showed an intermediate pattern, consisting in a moderate rise in CD8/CD4 ratio (Figure 5A).

Analysis of costimulatory receptor expression showed that all CAR T cell groups gradually down-regulated CD28 expression, more so in bone marrow but also in spleen (Figures S5B and S5C). In contrast, 4-1BB expression levels were sustained, especially in bone marrow (Figures S5B and S5C). The expression of exhaustion markers/inhibitory receptors PD-1, LAG-3 and TIM-3 was studied in all groups showing T cell persistence by week 3, namely 19BBz, 1928z-41BBL, 19BBz-CD80 and 19z1-CD80-41BBL (Figures 2 and 4). All three combinations designed to engage both CD28 and 4-1BB pathways showed reduced induction of PD-1, LAG-3 and TIM-3 relative to the second-generation 19BBz CAR (Figures 5B and 5C). While their cumulative expression was similar between the three former groups, it should be noted that 19BBz-CD80 T cells expressed the most PD-1, in bone marrow as well as in spleen (Figures 5B, 5C, S5D and S5E). The analysis of other T cell markers including KLRG1, CTLA4 and Fas showed less remarkable differences than the exhaustion markers (Figures S5F and S5G). No $CCR7^{+}CD62L^{+}CD45RA^{-}$ central memory T cells were detected 3 weeks after T cell infusion. Most persisting CAR T cells had a $CCR7^{-}CD62L^{-}CD45RA^{-}$ effector memory phenotype (Figures S5H and S5I).

Thus, the 1928z-41BBL configuration showed the most potent tumoricidal profile, increased T cell persistence, supported the highest CD8/CD4 ratio and induced the least PD-1 expression.

Combined CD28 and 4-1BB costimulation sustains IRF7/IFNβ pathway activation

To further understand the molecular mechanisms underlying the improved anti-tumor function induced by 1928z-41BBL, we performed genome wide gene expression profile of CD4 and CD8 1928z-41BBL T cells and compared it to 19z1-41BBL, 1928z and 19z1, which represent the elemental signaling modules within the design. We found that 35% of the top-20 up-regulated genes in 1928z-41BBL, are type-I interferon (IFN-I) targets. Analysis of curated pathway gene sets by Gene Set Enrichment Analysis (GSEA) (Subramanian et al., 2005) confirmed a highly statistically significant ($p<0.001$; FDR<0.001) enrichment of IFN-I pathway in both CD4 (Figure 6A) and CD8 (Figure 6B)

1928z-41BBL T cells. To evaluate the contribution of each individual signaling modality to the regulation of the IFN-I genes, we compared their expression in all four groups. We found that some of the IFN-I target genes were up-regulated in 19z1-41BBL T cells (Figures 6C and 6D), albeit to a lesser degree than in 1928z-41BBL T cells. Thus, combined CD28 and 4-1BB recruitment are required for potent induction of the IFN-I pathway. We validated the elevation of *IRF7*, *OAS1* and *IFI6* in both CD4 and CD8 1928z-41BBL T cells by real-time qPCR (Figure 6E). IRF7 is one of the main transcription factors regulating the IFN-I pathway (Honda et al., 2005; Sato et al., 1998). *IFNB1* transcripts markedly increased in 1928z-41BBL T cells 24 hr after antigen stimulation, compared to that of 1928z T cells, concomitantly with *IRF7* but not *IRF3* (Figure 6F). We did not detect *IFNA1* expression at any time point after antigen stimulation (data not shown). Importantly, *IRF7* and *IFNB1* expression were also induced in non-genetically modified human primary T cells stimulated with CD3/CD28 beads and 4-1BBL compared to CD3/CD28 bead stimulation alone (Figure S6), indicating that combined CD28/4-1BB costimulation triggers IFN-I signaling in human primary T cells independently of retroviral transduction and CAR expression. *IRF7* induction was confirmed in vivo in adoptively transferred T cells. Thus, ex vivo induction of *IRF7* and *IFNB1* expression was detected in the three constructs expressing costimulatory ligands, as well as 19BBz. Importantly, only 1928z-41BBL and 19BBz-CD80 sustained *IRF7* expression for at least three weeks in vivo (Figure 6G).

IRF7 induction augments the anti-tumor potential of CAR T cells

To assess the functional relevance of this induced IFN-I response in human T cells, we knocked down *IRF7* expression in 1928z-41BBL T cells, using two distinct shRNAs (IRF7sh1 or IRF7sh2) and a control shRNA (shK) (Figure S7A). Effective knockdown of *IRF7* resulted in a marked reduction in both *IFNB1* and *ISG15* induction (Figure 7A) as well as a reduction of IFNβ protein production (Figure 7B) in cultured T cells. To determine whether *IRF7* knockdown also had an effect on cytolytic potential, we measured IFNγ and granzyme-B production 18 hr after antigen exposure. Both were reduced, and comparable to levels measured in 1928z T cells stimulated under identical conditions (Figures 7C and S7B). Significantly, this deficit could be restored through addition of exogenous IFNβ (Figure 7D). To determine whether reduced *IRF7* impacted in vivo tumor rejection, we treated NALM6 bearing mice with 2×10^5 or 1×10^5 1928z-41BBL T cells expressing the control or anti-*IRF7* shRNAs. Tumor burden monitoring revealed that 1928z-41BBL T cells with reduced *IRF7* expression were compromised, allowing for continued tumor progression resulting in reduced overall survival, in contrast to 1928z-41BBL T cells expressing the control shRNA (Figures 7E and 7F). Reduction of *IRF7* expression did not significantly reduce accumulation of T cells in the bone marrow (Figure S7C) and blood (Figure S7D). In aggregate, these findings demonstrate that the primary impact of *IRF7* induction is to augment the anti-tumor function of adoptively transferred T cells, and that induction of *IRF7*, which is absent in 1928z T cells, plays an important role in the augmented anti-tumor activity of 1928z-41BBL T cells. Thus, the induction of the IRF7/IFNβ pathway, combined with the enhanced accumulation of 1928z-41BBL T cells, results in an improved balance between T cell functionality, proliferation and persistence, resulting in superior tumor eradication, which is evidenced at the lowest T cell infusion doses.

Discussion

The findings reported herein demonstrate the profound impact of optimizing engineered costimulation on the function of adoptively transferred T cells. Natural costimulation is a dynamic process that relies on a large number of costimulatory molecules, which are spatially and temporally recruited to achieve different functional outcomes (Chen and Flies, 2013; Miller and Sadelain, 2015). The genetic engineering of T cells is confined by technical limitations on the number of transduced or targeted genes, imposing a thoughtful analysis of which circuits to target and how to do so. CD28 and 4-1BB costimulatory domains have been the most widely used to date. The exact characteristics of CD28 and 4-1BB-based CARs have however not yet been fully expounded (van der Stegen et al., 2015).

Under stringent experimental conditions, we studied their relative potency in a xenogeneic model of ALL. This test reveals kinetic differences that are undetected at high treatment doses. Both CD28/CD3ζ and 4-1BB/CD3ζ-based CARs previously showed convincing anti-tumor efficacy and achieved high complete remission rates when used at high T cell doses, ranging between $5–20\times10^6$ CAR T cells (Brentjens et al., 2003; Kowolik et al., 2006; Brentjens et al., 2007; Milone et al., 2009; Lee et al., 2011; Tsukahara et al., 2013). We show here that clear differences in the kinetics of tumor control become apparent when lowering the T cell doses to $1–2\times10^5$ CAR T cells. Thus, both second generation CARs outperform the first generation 19z1 CAR, but they differ in their tumoricidal profile. 1928z T cells have greater anti-tumor activity, as reflected in more rapid tumor clearance. 19BBz T cells mediate slower tumor elimination, but can achieve similar tumor elimination owing to their greater persistence.

Recognizing these differential kinetics, we hypothesized that an ideal combination of both signals would preserve the superior tumoricidal capacity of CD28-based CARs with the sustenance afforded by the 4-1BB-based CARs. The converse hypothesis is that the two properties are antithetic and cannot be reconciled. We explored four engineering solutions relying on different structural conformations to engage T cell activation and costimulation. The combined recruitment of CD28 and 4-1BB costimulation proved to be highly sensitive to construct design. The 1928z-41BBL and 19BBz-CD80 configurations cumulate the most favorable properties in terms of in vivo tumoricidal cytotoxicity, proliferation, persistence and *IRF7* induction, although they still significantly differ. Thus, 1928z-41BBL directs more rapid tumor destruction than the 19BBz-CD80 configuration, reminiscent of the 1928z vs 19BBz comparison, while the added engagement of 4-1BB mediated by 4-1BBL extends the persistence to 1928z T cells. Although the 1928z-41BBL and 19BBz-CD80 T cell populations are similar in their induction of exhaustion markers and the induction of the IRF7/IFNβ pathway, they strikingly differ in the evolution of the CD8/CD4 ratio over time. 1928z-41BBL directs the highest and most sustained elevation of CD8 T cells. These combined features likely account for the emergence of 1928z-41BBL as the winner in terms of therapeutic efficacy in our “stress test”, resulting in complete remissions at doses of 1×10^5 and even 5×10^4 CAR T cells (data not shown).

The 1928BBz and 19z1-CD80-41BBL configurations were the least effective, albeit in different ways. 1928BBz directed robust early tumor reduction but T cells failed to expand,

while 19z1-CD80-41BBL expanded steadily but exerted inferior tumor control. Under the specific conditions of the model, the time interval to reach a CAR T cell to tumor ratio of 1:1, which is determined by both T cell expansion (quantity) and effector function (quality), serves as an indicator of T cell potency. The earlier this point is reached, the higher the efficacy of the therapy. No such ratio is ever attained with 19z1 CAR T cells. For 19z1-CD80-41BBL, this point is reached relatively late, reflecting a poor balance between effector and expansion functions. In the 5 remaining designs (1928z, 19BBz, 1928BBz, 1928z-41BBL and 19BBz-CD80), this point is reached by day 7, with 1928z-41BBL reaching the highest E:T ratio (117.5), followed by 1928z (14.7).

The “stress test” model shows that the 1928z-41BBL configuration captures all the features of rapid tumor elimination, sustained proliferation and increased T cell persistence. Furthermore, exhaustion markers are reduced in 1928z-41BBL T cells relative to 19BBz T cells. In aggregate, our findings suggest that lower T cell doses of 1928z-41BBL T cells will be needed in comparison to second generation CAR T cells, and that these T cells will display longer persistence and a higher CD8/CD4 ratio than obtained with either 1928z or 19BBz CAR therapy.

Providing costimulation in cis through the CAR or in trans through ligand/receptor interaction will result in spatial and temporal differences in the recruitment, kinetics and regulation of costimulation. Thus, the constitutive expression of CD80 on the T cell surface is not expected to be equivalent to the inclusion of the CD28 signaling domain within the CAR due to CTLA4 inhibition and receptor down-regulation. Other structural constraints bear on 4-1BB. The standard CAR design is a dimeric structure, whereas the natural conformation of activated 4-1BB is trimeric (van der Stegen et al., 2015), a structural difference that could affect downstream signaling efficacy (Park et al., 1999). In contrast, the use of 4-1BBL engages 4-1BB upon the latter’s induction to the T cell surface, which is structurally and kinetically distinct from the immediate 4-1BB clustering that occurs upon 19BBz binding to antigen.

At the molecular level, we conclude that 4-1BBL can effectively complement 1928z CAR activity owing to the sustained expression of 4-1BB over time, which contrasts with the gradually diminishing of CD28 expression, which averts the activity of its constitutively expressed ligand. Thus, 4-1BBL is more likely to find its cognate receptor than CD80, while 1928z may compensate for the loss of endogenous CD28, unlike 19BBz for endogenous 4-1BB. Additionally, the activity of CD80 may be further constrained by CTLA-4, which is not the case for the CD28 signal delivered through the 1928z CAR (Condomines et al., 2015). These differences in the engagement of CD28 and 4-1BB signaling pathways likely account for or contribute to the greater efficacy of 1928z-41BBL relative to 19BBz-CD80.

In aggregate, the findings reported herein support our hypothesis that optimized engagement of both CD28 and 4-1BB signals can reconcile the tumoricidal capacity of CD28-based CARs with the sustenance afforded by 4-1BB-based CARs, thereby resulting in enhanced CAR T cell potency. Furthermore, our data indicate that CD28 is the more powerful driver of an anti-tumor response, which is best delivered through a CD28/CD3ζ CAR, while the 4-1BB function is more productively coopted by coexpressing 4-1BBL along with a CD28/

CD3ζ CAR than by the converse design (19BBz-CD80), the fusion of CD28 and 4-1BB signaling domains (1928BBz), or the coexpression of both cotimulatory ligands (19z1-CD80-41BBL). The very distinct outcomes of these four CD28/4-1BB engineering conformations underscore the enormous sensitivity and subtlety of integrating costimulatory signals in activated T cells.

Our studies further reveal an *IRF7*-dependent activation of the T cell IFN-I response pathway. Whereas *IRF7* was transcribed following 4-1BB costimulation in CD4 T cells (and to a lesser extent in CD8 T cells), the persistence of its induction required combined CD28/4-1BB engagement. The delicate balance of optimal costimulation is again illustrated by the transient or delayed induction of *IRF7* and *IFNB1* in the less potent 19BBz and 19z1-CD80-41BBL T cells.

In addition to requiring activation and costimulatory signals, classically known as ‘Signal 1’ and ‘Signal 2’, respectively, the induction of an effective T cell response also relies on cytokine support, referred to as ‘Signal 3’. Signal 3 can support proliferation, clonal expansion, effector functions, and/or memory formation. A prominent example is type-I IFN which mediate CD8 T cell function (Curtsinger and Mescher, 2010). Type-I IFN is produced by many cell types, including dendritc cells (DCs) (Ivashkiv and Donlin, 2014; Stetson and Medzhitov, 2006). In this study, we found that human CAR T cells can produce significant levels of IFNβ, thereby supplying their own ‘Signal 3’. The ability of T cells to produce IFNβ was previously reported in mouse CD8 T cells only (Ysebrant de Lendonck et al., 2013). We show here that optimal augmentation of CD3ζ, CD28 and 4-1BB signaling in 1928z-41BBL T cells results in a durable activation of IRF7/IFNβ signal pathway, especially in CD4 T cells. This correlates with a stronger expansion of both CD4 and CD8 CAR T cells, resulting in enhanced tumor regression immediately after T cell injection.

The underlying mechanism(s) for mobilization of the IRF7/IFNβ pathway in T cells requires further examination. It is intriguing that 4-1BB signaling involves TRAF2 which provides CD28-independent costimulatory signals to resting T cells (Saoulli et al., 1998) and that TRAF2 might be involved in IFN-I gene induction (Sasai et al., 2010). There is also evidence that this signaling can induce IFNβ (Shin et al., 2006). Thus, the 4-1BB-TRAF2-IFN-I pathway may operate in 1928z-41BBL T cells. In this regard, although we did not see induction of mRNA for *IRF3*, which encodes the transcription factor that triggers the positive feedback loop of IFN-I induction by activating *IFNB1* in virally infected cells (Honda and Taniguchi, 2006), it is known that *IRF3* is constitutively expressed; hence, it is not excluded that *IRF3* is activated by 4-1BB signaling, thereby initiating the above described feedback loop. Obviously, further work will be required to address these issues.

Another interesting issue is the underlying mechanism(s) by which T cell-produced IFN-I exerts anti-tumor activities, which we infer to be complex. First, IFNβ produced at the site where CAR T cells recognize the malignant cells would exert its antitumor activities at locally high concentrations; it has been reported that IFN-I is cytotoxic to ALL (Manabe et al., 1993). Second, the activation of IRF7/IFNβ in 1928z-41BBL T cells augments two critical anti-tumor effector molecules, IFNγ and granzyme B, in both CD4 and CD8 T cells, wherein IFN-I in concert with T cell receptor stimulation robustly induces IFNγ in CD8 T

cells (Nguyen et al., 2002). Indeed, IFNγ is a key effector cytokine for T cell dependent tumor immunotherapy (Ngiow et al., 2011; Nishikawa et al., 2005; Wigginton et al., 2001). The potential anti-tumor effects of IFNγ are well documented, including direct anti-proliferative and pro-apoptotic effects on tumor cells (Chin et al., 1996; Ikeda et al., 2002), targeting of the tumor microenvironment through inhibition of angiogenesis (Ikeda et al., 2002) and stimulation of the innate and adaptive immune systems (Jaime-Ramirez et al., 2011; Ngiow et al., 2011; Nishikawa et al., 2005; Wigginton et al., 2001). Thirdly, IFN-I may regulate genes involved in CTL function by sustaining the expression of T-bet and Eomes as well as through chromatin remodeling (Agarwal et al., 2009; Lim et al., 2014) supporting the acquisition of better effector function (Hervas-Stubbs et al., 2010; Marshall et al., 2010; Mescher et al., 2006). Lastly, autocrine and paracrine IFN-I may inhibit regulatory T cells in the tumor microenvironment, thereby breaking cancer immune tolerance as reported in virally infected cells (Srivastava et al., 2014). We infer that these and possibly other mechanisms may be involved in an intricate manner in the clinical outcome of 1928z-41BBL T cell therapy. Thus, our current study sheds light on the classically known anti-tumor activity of IFN-I in cancer immunotherapy.

In addition to the vigorous tumoricidal function imparted by 1928z, 1928z-41BBL T cells are poised to promote tumor eradication through modulation of the tumor microenvironment in two ways. First, they facilitate targeted delivery of 4-1BB costimulation via the display of a costimulatory ligand on the T cell surface, resulting in trans-costimulation (Stephan et al., 2007). Second, the local delivery of IFNβ as “Signal 3” could enhance tumor eradication in multiple ways, by enhancing cross-priming activity of DCs (Diamond et al., 2011; Fuertes et al., 2011; Yang et al., 2014), inhibiting Treg activation and proliferation (Golding et al., 2010; Srivastava et al., 2014), and disrupting the tumor microvasculature (Spaapen et al., 2014). In a recent study, targeted delivery of IFNβ to the tumor site by an IFNβ-antibody fusion protein was shown to augment tumor antigen cross-presentation by CD8α DCs, activating CD8 T cells and inducing tumor remission (Yang et al., 2014). Thus, CD28/CD3ζ CAR T cells that co-express 4-1BBL are poised to recruit the host immune response against the tumor, potentially diversifying the antigen specificity of the immune response beyond the CAR target antigen and stimulating immunity that outlives the CAR T cells themselves. The findings we report here thus offer perspectives for T cell engineering in providing means to dial up or down effector functions, modulate T cell persistence and reprogram the tumor microenvironment through a constellation of effects afforded by the CAR T cell in trans. These properties are likely to be useful to tackle a broad range of cancers, including solid tumors.

Experimental Procedures

Retroviral vector constructs and retroviral production

Plasmids encoding the SFG γ-retroviral vector (Riviere et al., 1995) were prepared using standard molecular biology techniques. LNGFR is a truncated and mutated TNF-R family homolog (Gallardo et al., 1997) which was used as a control molecule to ensure comparable CAR expression levels from different bicistronic vectors. Synthesis of SFG- 19z1-LNGFR, SFG-1928z, SFG-19BBz and SFG-VexGFP has been previously described (Brentjens et al.,

2003; Brentjens et al., 2007; Maher et al., 2002). The SFG-19z1-LNGFR plasmid that includes a P2A bicistronic element was used as a template to obtain SFG-19z1-41BBL, 1928z-LNGFR and SFG-1928z-41BBL constructs. SFG-1928BBzhGFP was cloned from SFG-P28BBz-hGFP as previous described (Zhong et al., 2010). VSV-G pseudotyped retroviral supernatants derived from transduced gpg29 fibroblasts (H29) were used to construct stable retroviral producing cell lines using as previously described (Gong et al., 1999).

Human T cell cultures and retroviral transduction

Blood samples were obtained from healthy volunteers under an institutional review board-approved protocol, in accordance with the Declaration of Helsinki. PBMC were isolated by low-density centrifugation on Lymphoprep (Accurate Chemical and Scientific Corporation, Westbury, NY), activated with PHA for 48 hr and transduced on two consecutive days by centrifugation on retronectin-coated (Takara), oncoretroviral vector-bound plates. Alternatively, CD4 and CD8 T cells were first negatively purified by CD4 or CD8 T cell isolation kits (Miltenyi Biotec) and then positively selected and activated by CD3/CD28 beads (Invitrogen). Seven days after PHA or CD3/CD28-bead activation, transduced T cells were stained for transduction rate measurements and either injected to tumor-bearing mice or cocultured with irradiated confluent $CD19^+$ NIH 3T3s, at 10^6 cells/ml in 24-well tissue culture plates in RPMI medium supplemented with 10% FCS, with no added cytokines. Identical stimulations in fresh medium were performed weekly. Supernatants were harvested 24 hr after T cell stimulation for cytokine detection. Total cells were counted and CAR expression was weekly determined by flow cytometry.

Microarray procedure, gene expression analysis and Gene set enrichment analysis

Total RNA was extracted from three coculture replicates of CAR T cells, 20 hr after the second in vitro stimulation on 3T3s, using TRIzolTM Reagent (Invitrogen Life Technologies, Paisley, UK). RNA quality control parameters and microarray hybridization were performed at the MSKCC Genomics Core facility following the standard Illumina protocol (Illumina, San Diego, CA, USA). For gene expression analysis, we applied quantile normalization to raw data using the Partek Genomincs Suite. Differentially expressed genes among the four CAR T cells groups were determined by one-way repeated measures ANOVA ($p<0.01$) corrected by Benjamini-Hochberg's false discovery rate method ($p<0.05$). Heatmaps were performed in Partek Genomincs Suite using normalized data standardized on average. The complete data was deposited in the NCBI Gene Expression Omnibus under accession number GSE68329. The Gene Set Enrichment Analysis, GSEA, (Subramanian et al., 2005) was performed on curated pathway gene sets from the Broad Molecular Signature Database (http://www.broadinstitute.org/gsea/msigdb/).

Mouse systemic tumor model

We used 8–12 week old NOD.Cg-Prkdc^{scid}Il2rg^{tm1Wjl}/SzJ (NSG) mice (Jackson Laboratory), under a protocol approved by the MSKCC Institutional Animal Care and Use Committee. Mice were inoculated with 0.5×10^6 FFLuc-GFP NALM6 cells by tail vein injection followed by 1 to 4×10^5 CAR T cells four days later. NALM6 produce very even tumor burdens and no mice were excluded prior to treatment. No blinding method was used.

Bioluminescence imaging utilized the Xenogen IVIS Imaging System (Xenogen) with Living Image software (Xenogen) for acquisition of imaging data sets. Tumor burden was assessed as previously described (Gade et al., 2005).

T cell and tumor cell isolation from bone marrow and spleen

For qPCR assay, CAR T cells were first negatively enriched by Dynabeads mouse untouched T cells (Invitrogen) and human CD19 Beads (Miltenyi Biotec) and subsequently positively purified using Dynabeads human CD3 (Invitrogen). For the cytotoxicity assay, CAR T cells were only negatively purified.

Statistical Analyses

Data were analyzed using Prism 5.0 (GraphPad Software, Inc.). Statistical comparisons between two groups were determined by Student's *t* tests. All p values are two-tailed. The Log-rank test was used to compare survival curves obtained with Kaplan-Meier method. For the in vivo studies, no pre-specified effect size was used to determine sample sizes. The use of statistical tests was chosen according to the nature of the data. Comparison of survival curves was done using the log-rank test. Statistical significance was defined as $p<0.05$.

Supplementary Material

Refer to Web version on PubMed Central for supplementary material.

Acknowledgments

We thank Drs Isabelle Rivière (MSKCC) and Jorge Mansilla-Soto (MSKCC) for helpful discussion, and Dr Tadatsugu Taniguchi (Institute of Industrial Science, University of Tokyo) for critical review of our discussion. We thank the SKI Genomics core facility for technical help in microarray analysis and the SKI Flow Cytometry core facility for cell sorting. This work was funded by the MSKCC Center for Cell Engineering (Lewis Sanders Fund), the MSKCC Experimental Therapeutics Center (ETC), the Cancer Research Institute (CRI), the Mallah fund, the Lake Road Foundation, the Mr. William H. and Mrs. Alice Goodwin and the Commonwealth Foundation for Cancer Research and Stand Up To Cancer/AACR. Stand Up To Cancer is a program of the Entertainment Industry Foundation administered by the American Association for Cancer Research. M.C. was initially supported by a post-doctoral Fellowship from the Association pour la Recherche contre le Cancer (ARC).

References

Agarwal P, Raghavan A, Nandiwada SL, Curtsinger JM, Bohjanen PR, Mueller DL, Mescher MF. Gene regulation and chromatin remodeling by IL-12 and type I IFN in programming for CD8 T cell effector function and memory. Journal of immunology. 2009; 183:1695–1704.

Brentjens RJ, Latouche JB, Santos E, Marti F, Gong MC, Lyddane C, King PD, Larson S, Weiss M, Riviere I, Sadelain M. Eradication of systemic B-cell tumors by genetically targeted human T lymphocytes co-stimulated by CD80 and interleukin-15. Nature medicine. 2003; 9:279–286.

Brentjens RJ, Riviere I, Park JH, Davila ML, Wang X, Stefanski J, Taylor C, Yeh R, Bartido S, Borquez-Ojeda O, et al. Safety and persistence of adoptively transferred autologous CD19-targeted T cells in patients with relapsed or chemotherapy refractory B-cell leukemias. Blood. 2011; 118:4817–4828. [PubMed: 21849486]

Brentjens RJ, Santos E, Nikhamin Y, Yeh R, Matsushita M, La Perle K, Quintas-Cardama A, Larson SM, Sadelain M. Genetically targeted T cells eradicate systemic acute lymphoblastic leukemia xenografts. Clinical cancer research : an official journal of the American Association for Cancer Research. 2007; 13:5426–5435. [PubMed: 17855649]

Carpenito C, Milone MC, Hassan R, Simonet JC, Lakhal M, Suhoski MM, Varela-Rohena A, Haines KM, Heitjan DF, Albelda SM, et al. Control of large, established tumor xenografts with genetically

retargeted human T cells containing CD28 and CD137 domains. Proceedings of the National Academy of Sciences of the United States of America. 2009; 106:3360–3365. [PubMed: 19211796]

Chen L, Flies DB. Molecular mechanisms of T cell co-stimulation and co-inhibition. Nature reviews Immunology. 2013; 13:227–242.

Chin YE, Kitagawa M, Su WC, You ZH, Iwamoto Y, Fu XY. Cell growth arrest and induction of cyclin-dependent kinase inhibitor p21 WAF1/CIP1 mediated by STAT1. Science. 1996; 272:719–722. [PubMed: 8614832]

Condomines M, Arnason J, Benjamin R, Gunset G, Plotkin J, Sadelain M. Tumor-Targeted Human T Cells Expressing CD28-Based Chimeric Antigen Receptors Circumvent CTLA-4 Inhibition. PloS one. 2015; 10:e0130518. [PubMed: 26110267]

Curtsinger JM, Mescher MF. Inflammatory cytokines as a third signal for T cell activation. Current opinion in immunology. 2010; 22:333–340. [PubMed: 20363604]

Davila ML, Brentjens R, Wang X, Riviere I, Sadelain M. How do CARs work?: Early insights from recent clinical studies targeting CD19. Oncoimmunology. 2012; 1:1577–1583. [PubMed: 23264903]

Davila ML, Riviere I, Wang X, Bartido S, Park J, Curran K, Chung SS, Stefanski J, Borquez-Ojeda O, Olszewska M, et al. Efficacy and toxicity management of 19–28z CAR T cell therapy in B cell acute lymphoblastic leukemia. Science translational medicine. 2014; 6:224ra225.

Diamond MS, Kinder M, Matsushita H, Mashayekhi M, Dunn GP, Archambault JM, Lee H, Arthur CD, White JM, Kalinke U, et al. Type I interferon is selectively required by dendritic cells for immune rejection of tumors. The Journal of experimental medicine. 2011; 208:1989–2003. [PubMed: 21930769]

Fuertes MB, Kacha AK, Kline J, Woo SR, Kranz DM, Murphy KM, Gajewski TF. Host type I IFN signals are required for antitumor CD8+ T cell responses through CD8{alpha}+ dendritic cells. The Journal of experimental medicine. 2011; 208:2005–2016. [PubMed: 21930765]

Gade TP, Hassen W, Santos E, Gunset G, Saudemont A, Gong MC, Brentjens R, Zhong XS, Stephan M, Stefanski J, et al. Targeted elimination of prostate cancer by genetically directed human T lymphocytes. Cancer research. 2005; 65:9080–9088. [PubMed: 16204083]

Gallardo HF, Tan C, Sadelain M. The internal ribosomal entry site of the encephalomyocarditis virus enables reliable coexpression of two transgenes in human primary T lymphocytes. Gene therapy. 1997; 4:1115–1119. [PubMed: 9415319]

Golding A, Rosen A, Petri M, Akhter E, Andrade F. Interferon-alpha regulates the dynamic balance between human activated regulatory and effector T cells: implications for antiviral and autoimmune responses. Immunology. 2010; 131:107–117. [PubMed: 20465564]

Gong MC, Latouche JB, Krause A, Heston WD, Bander NH, Sadelain M. Cancer patient T cells genetically targeted to prostate-specific membrane antigen specifically lyse prostate cancer cells and release cytokines in response to prostate-specific membrane antigen. Neoplasia. 1999; 1:123–127. [PubMed: 10933046]

Grupp SA, Kalos M, Barrett D, Aplenc R, Porter DL, Rheingold SR, Teachey DT, Chew A, Hauck B, Wright JF, et al. Chimeric antigen receptor-modified T cells for acute lymphoid leukemia. The New England journal of medicine. 2013; 368:1509–1518. [PubMed: 23527958]

Hervas-Stubbs S, Riezu-Boj JI, Gonzalez I, Mancheno U, Dubrot J, Azpilicueta A, Gabari I, Palazon A, Aranguren A, Ruiz J, et al. Effects of IFN-alpha as a signal-3 cytokine on human naive and antigen-experienced CD8(+) T cells. European journal of immunology. 2010; 40:3389–3402. [PubMed: 21108462]

Ho WY, Blattman JN, Dossett ML, Yee C, Greenberg PD. Adoptive immunotherapy: engineering T cell responses as biologic weapons for tumor mass destruction. Cancer cell. 2003; 3:431–437. [PubMed: 12781360]

Honda K, Taniguchi T. IRFs: master regulators of signalling by Toll-like receptors and cytosolic pattern-recognition receptors. Nature reviews Immunology. 2006; 6:644–658.

Honda K, Yanai H, Negishi H, Asagiri M, Sato M, Mizutani T, Shimada N, Ohba Y, Takaoka A, Yoshida N, Taniguchi T. IRF-7 is the master regulator of type-I interferon-dependent immune responses. Nature. 2005; 434:772–777. [PubMed: 15800576]

Ikeda H, Old LJ, Schreiber RD. The roles of IFN gamma in protection against tumor development and cancer immunoediting. Cytokine & growth factor reviews. 2002; 13:95–109. [PubMed: 11900986]

Imai C, Mihara K, Andreansky M, Nicholson IC, Pui CH, Geiger TL, Campana D. Chimeric receptors with 4-1BB signaling capacity provoke potent cytotoxicity against acute lymphoblastic leukemia. Leukemia. 2004; 18:676–684. [PubMed: 14961035]

Ivashkiv LB, Donlin LT. Regulation of type I interferon responses. Nature reviews Immunology. 2014; 14:36–49.

Jaime-Ramirez AC, Mundy-Bosse BL, Kondadasula S, Jones NB, Roda JM, Mani A, Parihar R, Karpa V, Papenfuss TL, LaPerle KM, et al. IL-12 enhances the antitumor actions of trastuzumab via NK cell IFN-gamma production. Journal of immunology. 2011; 186:3401–3409.

Kowolik CM, Topp MS, Gonzalez S, Pfeiffer T, Olivares S, Gonzalez N, Smith DD, Forman SJ, Jensen MC, Cooper LJ. CD28 costimulation provided through a CD19-specific chimeric antigen receptor enhances in vivo persistence and antitumor efficacy of adoptively transferred T cells. Cancer research. 2006; 66:10995–11004. [PubMed: 17108138]

Lee DW, Kochenderfer JN, Stetler-Stevenson M, Cui YK, Delbrook C, Feldman SA, Fry TJ, Orentas R, Sabatino M, Shah NN, et al. T cells expressing CD19 chimeric antigen receptors for acute lymphoblastic leukaemia in children and young adults: a phase 1 dose-escalation trial. Lancet. 2015; 385:517–528. [PubMed: 25319501]

Lee JC, Hayman E, Pegram HJ, Santos E, Heller G, Sadelain M, Brentjens R. In vivo inhibition of human CD19-targeted effector T cells by natural T regulatory cells in a xenotransplant murine model of B cell malignancy. Cancer research. 2011; 71:2871–2881. [PubMed: 21487038]

Lim JY, Gerber SA, Murphy SP, Lord EM. Type I interferons induced by radiation therapy mediate recruitment and effector function of CD8(+) T cells. Cancer immunology, immunotherapy : CII. 2014; 63:259–271. [PubMed: 24357146]

Maher J, Brentjens RJ, Gunset G, Riviere I, Sadelain M. Human T-lymphocyte cytotoxicity and proliferation directed by a single chimeric TCRzeta /CD28 receptor. Nature biotechnology. 2002; 20:70–75.

Manabe A, Yi T, Kumagai M, Campana D. Use of stroma-supported cultures of leukemic cells to assess antileukemic drugs. I. Cytotoxicity of interferon alpha in acute lymphoblastic leukemia. Leukemia. 1993; 7:1990–1995. [PubMed: 8255098]

Marshall HD, Prince AL, Berg LJ, Welsh RM. IFN-alpha beta and self-MHC divert CD8 T cells into a distinct differentiation pathway characterized by rapid acquisition of effector functions. Journal of immunology. 2010; 185:1419–1428.

Maude SL, Frey N, Shaw PA, Aplenc R, Barrett DM, Bunin NJ, Chew A, Gonzalez VE, Zheng Z, Lacey SF, et al. Chimeric antigen receptor T cells for sustained remissions in leukemia. The New England journal of medicine. 2014; 371:1507–1517. [PubMed: 25317870]

Mescher MF, Curtsinger JM, Agarwal P, Casey KA, Gerner M, Hammerbeck CD, Popescu F, Xiao Z. Signals required for programming effector and memory development by CD8+ T cells. Immunological reviews. 2006; 211:81–92. [PubMed: 16824119]

Miller JF, Sadelain M. The journey from discoveries in fundamental immunology to cancer immunotherapy. Cancer cell. 2015; 27:439–449. [PubMed: 25858803]

Milone MC, Fish JD, Carpenito C, Carroll RG, Binder GK, Teachey D, Samanta M, Lakhal M, Gloss B, Danet-Desnoyers G, et al. Chimeric receptors containing CD137 signal transduction domains mediate enhanced survival of T cells and increased antileukemic efficacy in vivo. Molecular therapy : the journal of the American Society of Gene Therapy. 2009; 17:1453–1464. [PubMed: 19384291]

Ngiow SF, von Scheidt B, Akiba H, Yagita H, Teng MW, Smyth MJ. Anti-TIM3 antibody promotes T cell IFN-gamma-mediated antitumor immunity and suppresses established tumors. Cancer research. 2011; 71:3540–3551. [PubMed: 21430066]

Nishikawa H, Kato T, Tawara I, Ikeda H, Kuribayashi K, Allen PM, Schreiber RD, Old LJ, Shiku H. IFN-gamma controls the generation/activation of CD4+ CD25+ regulatory T cells in antitumor immune response. Journal of immunology. 2005; 175:4433–4440.

Nguyen KB, Watford WT, Salomon R, Hofmann SR, Pien GC, Morinobu A, Gadina M, O'Shea JJ, Biron CA. Critical role for STAT4 activation by type 1 interferons in the interferon-gamma response to viral infection. Science. 2002; 297:2063–2066. [PubMed: 12242445]

Park YC, Burkitt V, Villa AR, Tong L, Wu H. Structural basis for self-association and receptor recognition of human TRAF2. Nature. 1999; 398:533–538. [PubMed: 10206649]

Ramos CA, Savoldo B, Dotti G. CD19-CAR trials. Cancer journal. 2014; 20:112–118.

Riviere I, Brose K, Mulligan RC. Effects of retroviral vector design on expression of human adenosine deaminase in murine bone marrow transplant recipients engrafted with genetically modified cells. Proceedings of the National Academy of Sciences of the United States of America. 1995; 92:6733–6737. [PubMed: 7624312]

Sadelain M. CAR therapy: the CD19 paradigm. The Journal of clinical investigation. 2015 *in press*.

Sadelain M, Brentjens R, Riviere I. The promise and potential pitfalls of chimeric antigen receptors. Current opinion in immunology. 2009; 21:215–223. [PubMed: 19327974]

Saoulli K, Lee SY, Cannons JL, Yeh WC, Santana A, Goldstein MD, Bangia N, DeBenedette MA, Mak TW, Choi Y, Watts TH. CD28-independent, TRAF2-dependent costimulation of resting T cells by 4-1BB ligand. The Journal of experimental medicine. 1998; 187:1849–1862. [PubMed: 9607925]

Sasai M, Tatematsu M, Oshiumi H, Funami K, Matsumoto M, Hatakeyama S, Seya T. Direct binding of TRAF2 and TRAF6 to TICAM-1/TRIF adaptor participates in activation of the Toll-like receptor 3/4 pathway. Molecular immunology. 2010; 47:1283–1291. [PubMed: 20047764]

Sato M, Hata N, Asagiri M, Nakaya T, Taniguchi T, Tanaka N. Positive feedback regulation of type I IFN genes by the IFN-inducible transcription factor IRF-7. FEBS letters. 1998; 441:106–110. [PubMed: 9877175]

Shin HH, Lee EA, Kim SJ, Kwon BS, Choi HS. A signal through 4-1BB ligand inhibits receptor for activation of nuclear factor-kappaB ligand (RANKL)-induced osteoclastogenesis by increasing interferon (IFN)-beta production. FEBS letters. 2006; 580:1601–1606. [PubMed: 16480981]

Spaapen RM, Leung MY, Fuertes MB, Kline JP, Zhang L, Zheng Y, Fu YX, Luo X, Cohen KS, Gajewski TF. Therapeutic activity of high-dose intratumoral IFN-beta requires direct effect on the tumor vasculature. Journal of immunology. 2014; 193:4254–4260.

Srivastava S, Koch MA, Pepper M, Campbell DJ. Type I interferons directly inhibit regulatory T cells to allow optimal antiviral T cell responses during acute LCMV infection. The Journal of experimental medicine. 2014; 211:961–974. [PubMed: 24711580]

Stephan MT, Ponomarev V, Brentjens RJ, Chang AH, Dobrenkov KV, Heller G, Sadelain M. T cell-encoded CD80 and 4-1BBL induce auto- and transcostimulation, resulting in potent tumor rejection. Nature medicine. 2007; 13:1440–1449.

Stetson DB, Medzhitov R. Type I interferons in host defense. Immunity. 2006; 25:373–381. [PubMed: 16979569]

Subramanian A, Tamayo P, Mootha VK, Mukherjee S, Ebert BL, Gillette MA, Paulovich A, Pomeroy SL, Golub TR, Lander ES, Mesirov JP. Gene set enrichment analysis: a knowledge-based approach for interpreting genome-wide expression profiles. Proceedings of the National Academy of Sciences of the United States of America. 2005; 102:15545–15550. [PubMed: 16199517]

Tammana S, Huang X, Wong M, Milone MC, Ma L, Levine BL, June CH, Wagner JE, Blazar BR, Zhou X. 4-1BB and CD28 signaling plays a synergistic role in redirecting umbilical cord blood T cells against B-cell malignancies. Human gene therapy. 2010; 21:75–86. [PubMed: 19719389]

Tsukahara T, Ohmine K, Yamamoto C, Uchibori R, Ido H, Teruya T, Urabe M, Mizukami H, Kume A, Nakamura M, et al. CD19 target-engineered T-cells accumulate at tumor lesions in human B-cell lymphoma xenograft mouse models. Biochemical and biophysical research communications. 2013; 438:84–89. [PubMed: 23872144]

van der Stegen SJ, Hamieh M, Sadelain M. The pharmacology of second-generation chimeric antigen receptors. Nature reviews Drug discovery. 2015; 14:499–509. [PubMed: 26129802]

Wigginton JM, Gruys E, Geiselhart L, Subleski J, Komschlies KL, Park JW, Wiltrout TA, Nagashima K, Back TC, Wiltrout RH. IFN-gamma and Fas/FasL are required for the antitumor and antiangiogenic effects of IL-12/pulse IL-2 therapy. The Journal of clinical investigation. 2001; 108:51–62. [PubMed: 11435457]

Yang X, Zhang X, Fu ML, Weichselbaum RR, Gajewski TF, Guo Y, Fu YX. Targeting the tumor microenvironment with interferon-beta bridges innate and adaptive immune responses. Cancer cell. 2014; 25:37–48. [PubMed: 24434209]

Ysebrant de Lendonck L, Tonon S, Nguyen M, Vandevenne P, Welsby I, Martinet V, Molle C, Charbonnier LM, Leo O, Goriely S. Interferon regulatory factor 3 controls interleukin-17 expression in CD8 T lymphocytes. Proceedings of the National Academy of Sciences of the United States of America. 2013; 110:E3189–E3197. [PubMed: 23918362]

Zhao Y, Wang QJ, Yang S, Kochenderfer JN, Zheng Z, Zhong X, Sadelain M, Eshhar Z, Rosenberg SA, Morgan RA. A herceptin-based chimeric antigen receptor with modified signaling domains leads to enhanced survival of transduced T lymphocytes and antitumor activity. Journal of immunology. 2009; 183:5563–5574.

Zhong XS, Matsushita M, Plotkin J, Riviere I, Sadelain M. Chimeric antigen receptors combining 4-1BB and CD28 signaling domains augment PI3kinase/AKT/Bcl-XL activation and CD8+ T cell-mediated tumor eradication. Molecular therapy : the journal of the American Society of Gene Therapy. 2010; 18:413–420. [PubMed: 19773745]

Significance

CAR T cells are a promising immunotherapeutic approach for B cell malignancies. Second generation CARs utilizing either CD28 or 4-1BB signaling domains have resulted in dramatic clinical responses, especially in patients with refractory acute lymphoblastic leukemia. We reveal here the different kinetics of these CARs, and demonstrate that their respective advantages can be reconciled with adept receptor and ligand engineering. T cells receiving integrated CD28 and 4-1BB signals display superior tumoricidal activity and robust persistence. These T cells also activate the IRF7/IFNβ pathway, which supports the anti-tumor activity of these T cells. Thus, CAR T cells can be engineered to different levels of potency, which may be useful to tackle a broad range of cancers, including solid tumors.

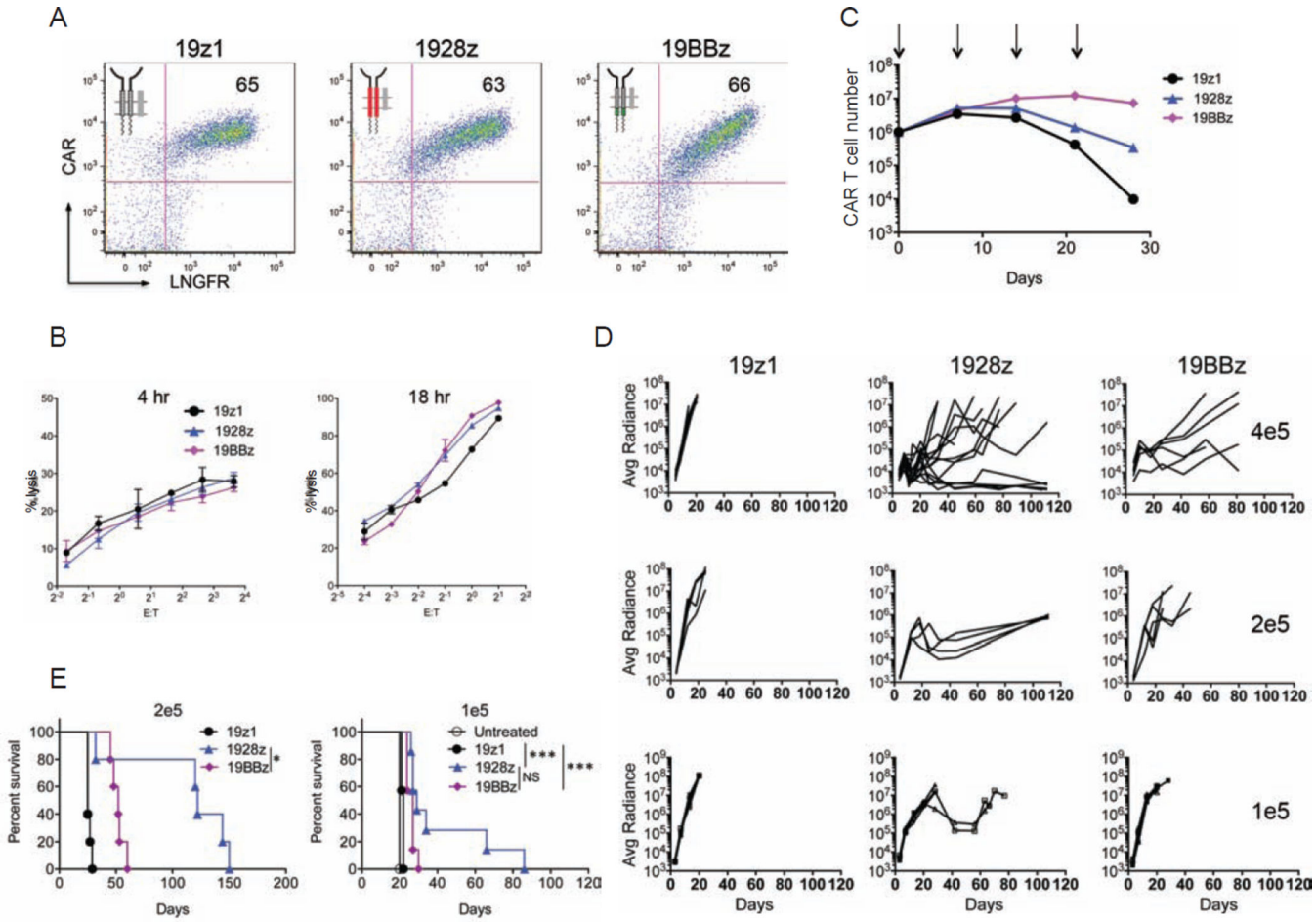

Figure 1. Therapeutic potency of first and second-generation CAR designs

One first generation, 19z1, and two second-generation CD19-specific CARs, 1928z and 19BBz, were compared for their anti-tumor effect in a systemic NALM/6 model. (**A**) Flow cytometric analysis showing CAR and LNGFR expression. (**B**) Cytotoxic activity using a 4 hr ^{51}Cr release assay (left) and an 18 hr bioluminescence assay (right), utilizing NALM6 as targets cells. Data are means ± SD. (**C**) Cumulative cell counts of indicated CAR T cells upon weekly CD19 stimulation, without exogenous cytokines. Arrows indicate stimulation time points. Data are means ± SD. (**D**) NALM6 bearing mice were treated with 4×10^5 (**top**), 2×10^5 (**middle**) or 1×10^5 (**bottom**) indicated CAR T cells. Tumor burden shown as bioluminescent signal quantified per animal every week over a 120-day period. Quantification is the average photon count of ventral and dorsal acquisitions per animal at all given time points. Each line represents one mouse. Some groups are pooled from at least two experiments, representing n=5–14 mice per group. (**E**) Kaplan-Meier analysis of survival of mice in (**D**). *p<0.05; **p<0.01; ***p<0.001. See also Figure S1.

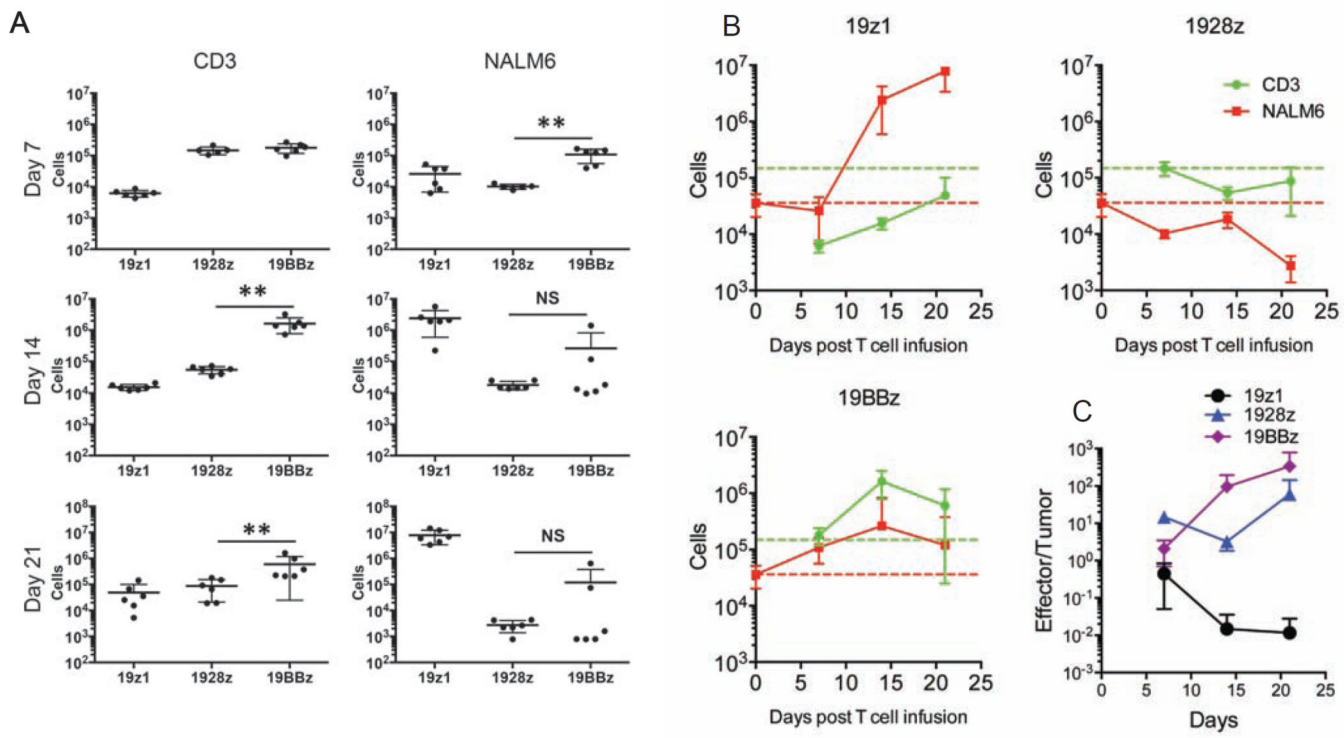

Figure 2. In vivo T cell accumulation and tumor burden kinetics of first and second generation CAR designs

NALM6 bearing mice were treated with 2×10^5 indicated CAR T cells. One, two and three weeks after CAR T cell infusion, mice were sacrificed and bone marrow cells were harvested. CAR T cells and NALM6 cells were analyzed and counted by flow cytometry. (**A**) Each dot represents one mouse, *p<0.05; **p<0.01. (**B**) Each line represents n=6 mice per group per timepoint. Red and green broken line respectively indicate NALM6 cell number at the time of T cell infusion and 1928z T cell accumulation at day 7. (**C**) Effector/Tumor (CAR T/NALM6) ratios were shown at different time points. All data are means ± SD. See also Figure S2.

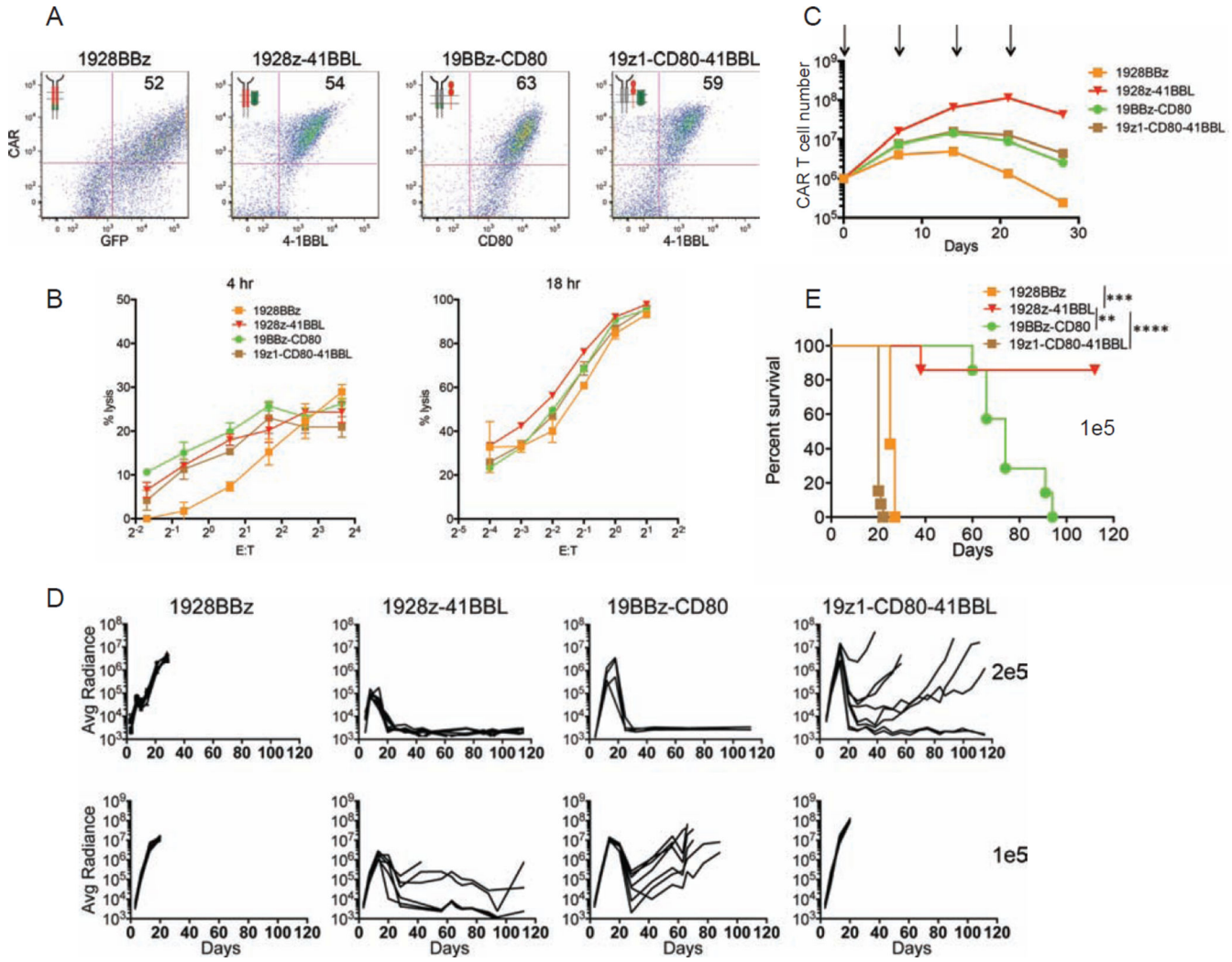

Figure 3. Therapeutic potency of a third generation CAR and three alternative combinations of costimulatory CAR designs

(**A**) Flow cytometric analysis showing expression levels of the indicated CARs. (**B**) Cytotoxic activity using a 4 hr ^{51}Cr release assay (left) and 18 hr bioluminescence assay (right), utilizing NALM6 cell line as targets cells. Data are means ± SD. (**C**) Cumulative CAR T cell counts of indicated CAR T cells upon weekly CD19 stimulation, without exogenous cytokines. Arrows indicate stimulation time points. Data are means ± SD. (**D**) NALM6 bearing mice were treated with 2×10^5 (**top**), or 1×10^5 (**bottom**) indicated CAR T cells. Tumor burden showed as the bioluminescent signal quantified per animal every week over a 120-day period. Quantification is the average photon count of ventral and dorsal acquisitions per animal at all given time points. Each line represents one mouse. Some groups are pooled from at least two experiments, representing n=7–14 mice per group. (**E**) Kaplan-Meier analysis of survival of mice in (**D**). *p<0.05; **p<0.01; ***p<0.001. See also Figure S3.

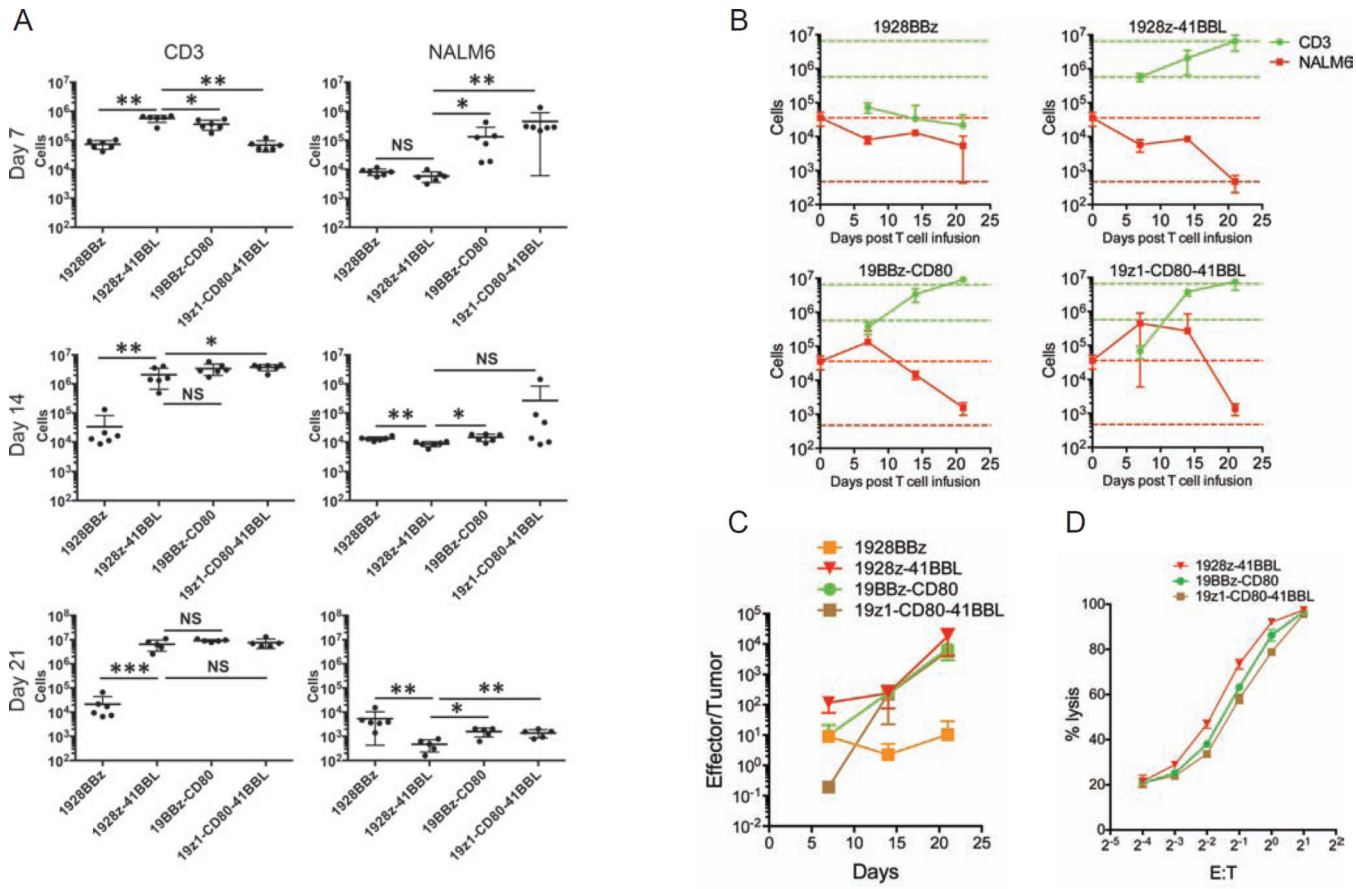

Figure 4. In vivo T cell accumulation and tumor burden kinetics of a third generation and different combinations of costimulatory CAR designs

NALM6 bearing mice were treated with 2×10^5 indicated CAR T cells. One, two and three weeks after CAR T cell infusion, mice were sacrificed and bone marrow cells were harvested from two femurs. CAR T cells and NALM6 cells were analyzed and counted by flow cytometry. (**A**) Each dot represents one mouse, *p<0.05; **p<0.01. (**B**) Each line represents n=6 mice per group per timepoint. Red and green broken line respectively indicate NALM6 cell number at the time of T cell infusion and 1928z-41BBL T cell accumulation at day 7 and 21. (**C**) Effector/Tumor (CAR T/NALM6) ratios were shown at different time points. (**D**) Cytotoxic activity of indicated ex vivo CAR T cells as shown using an 18 hr bioluminescence assay, utilizing NALM6 cell line as targets cells. CAR T cells were isolated from mouse spleens 3 weeks after treatment and pooled from 5–6 mice. All data are means ± SD. See also Figure S4.

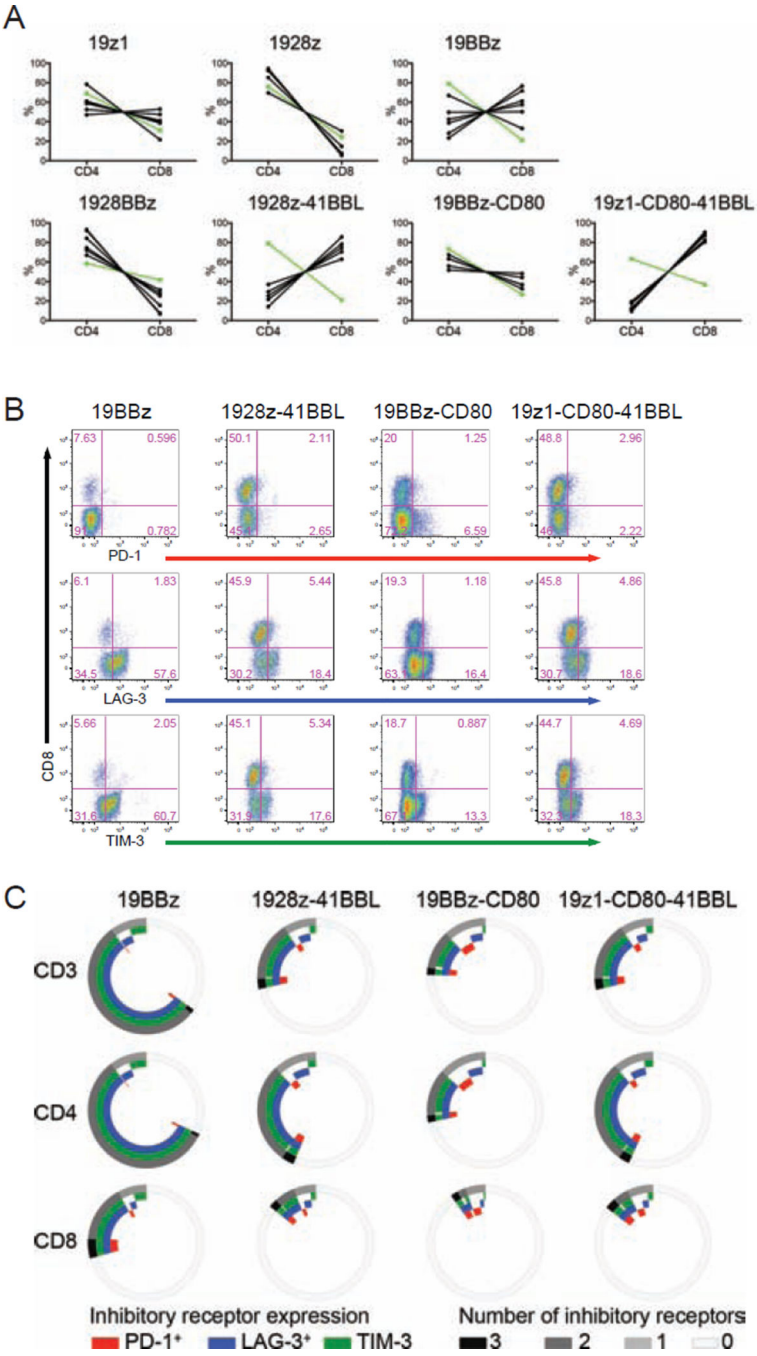

Figure 5. Optimally combined 4-1BB and CD28 costimulation promotes higher CD8/CD4 ratios and reduces T cell exhaustion

NALM6 bearing mice were treated with 2×10^5 of indicated CAR T cells. Three weeks after CAR T cell infusion, mice were sacrificed and bone marrow cells were harvested from two femurs. CD4 and CD8 CAR T cells were analyzed and counted by flow cytometry. **(A)** CD4 and CD8 CAR T cell percentage in each mouse of indicated CAR design. Each black line represents one mouse. The green line represents the initial ratio at the time of infusion. (**B**)

FACS plots showing PD-1, LAG-3, TIM-3 expression. (**C**) Exhaustion marker analysis of B. See also Figure S5.

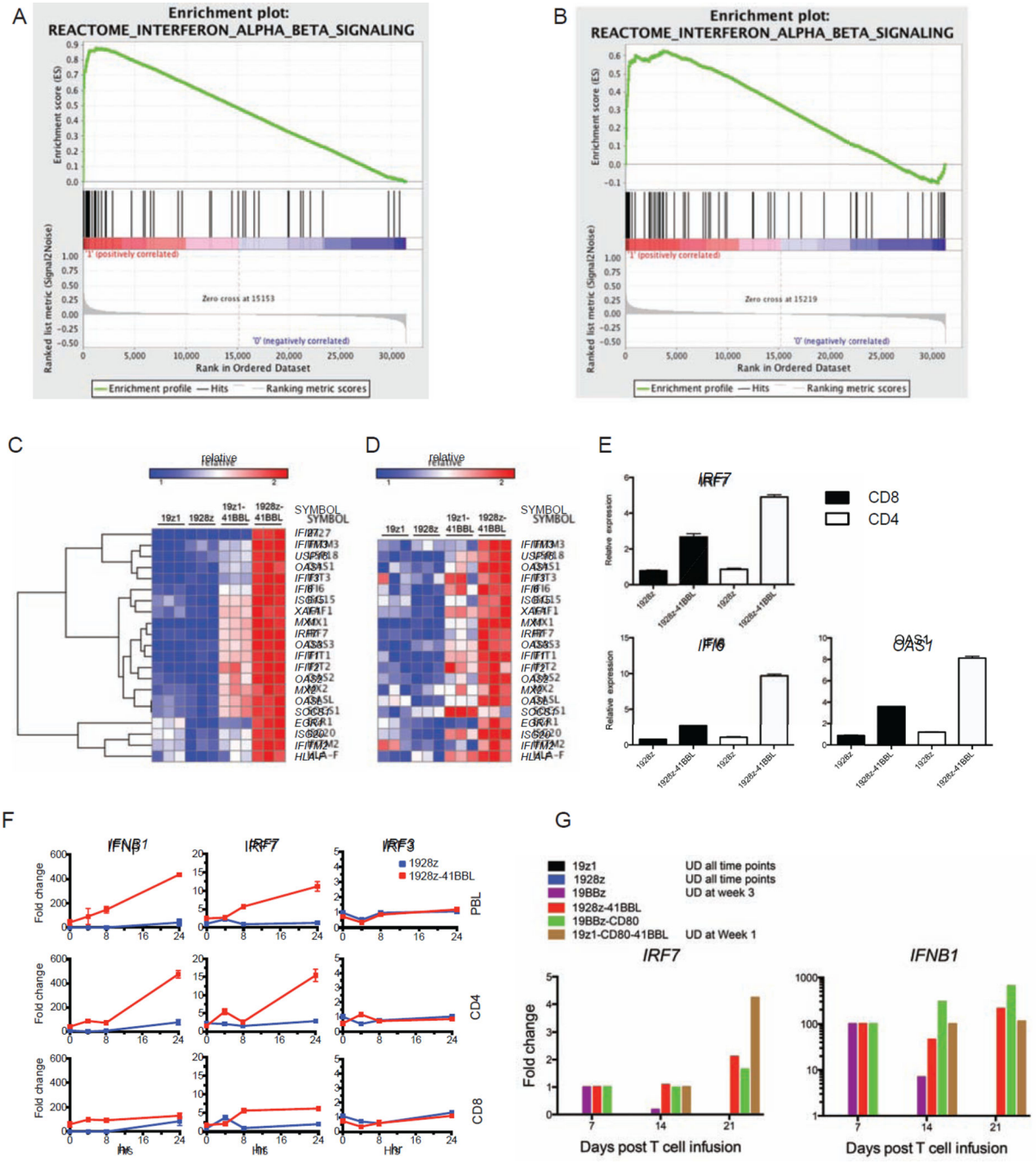

Figure 6. Antigen activation combined with CD28 and 4-1BB costimulation induces strong intrinsic activation of the type I IFN pathway in human T cells

Gene expression profiles were analyzed in stimulated CD4 or CD8 CAR T cells at day 15 in culture. **(A)** GSEA analysis showing the enrichment of type I IFN signaling, in 1928z-41BBL versus 19z1 CD4 CAR cells. **(B)** Same GSEA analysis in CD8 CAR T cells. **(C)** Expression levels of type I IFN genes in indicated CD4 CAR T cells. **(D)** Expression levels of type I IFN genes in indicated CD8 CAR T cells. (**E**) Relative expression of *IRF7* and two ISGs (*OAS1* and *IFI6*), using qPCR for indicated CAR T cells. Data are means ±

SD. **(F)** Relative expression of *IFNB1*, *IRF7* and *IRF3* at indicated time points after stimulation, measured by qPCR in indicated CAR T cells generated from unselected lymphocytes (PBLs), highly purified CD4 or CD8 T cells. Data are means ± SD. **(G)** Relative expression of *IRF7 and IFNB1* at indicated time points measured by qPCR in purified ex vivo CAR T cell as described in Figures 2A and 4A. Each group was normalized to its first detectable expression level. See also Figure S6.

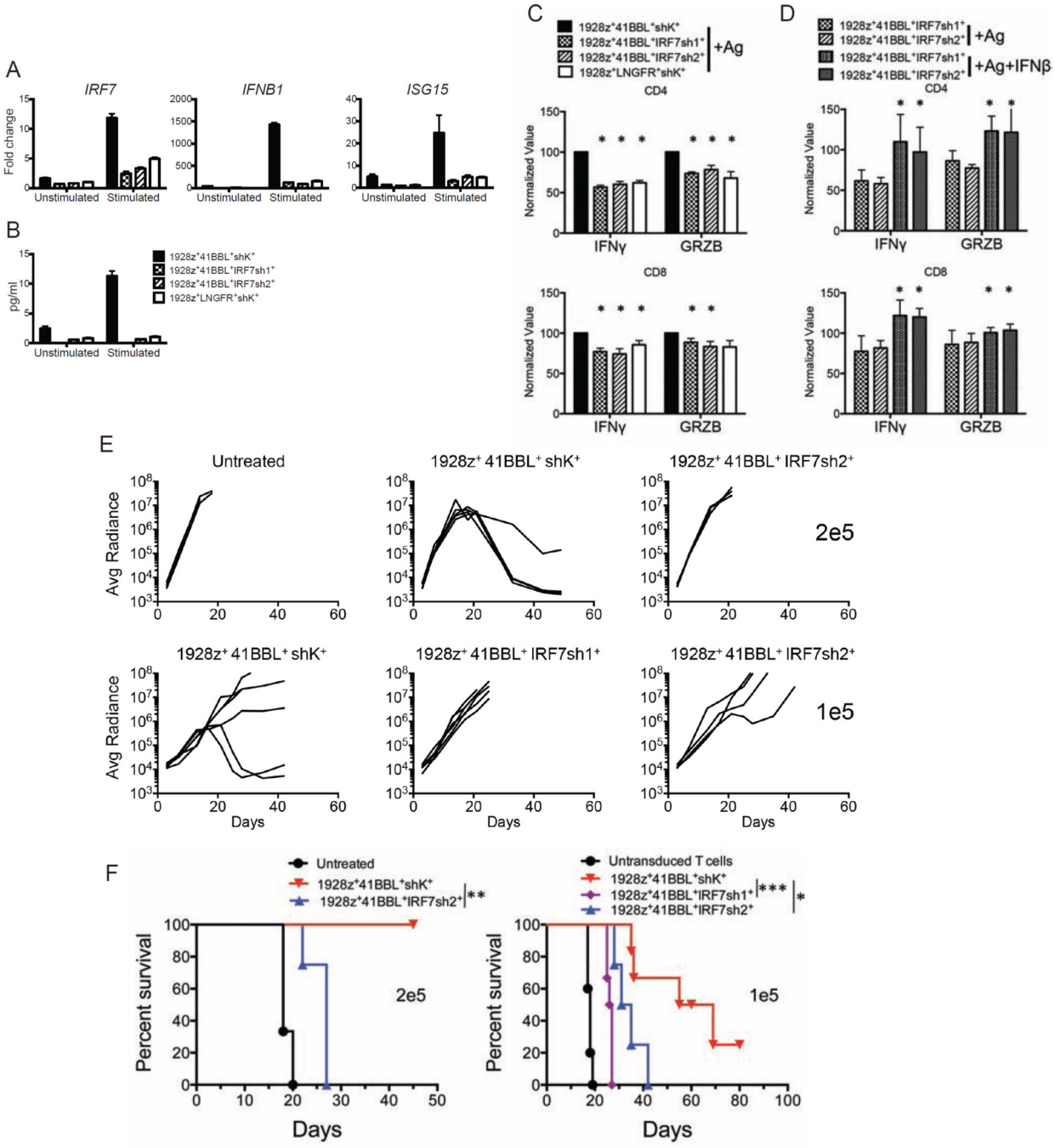

Figure 7. *IRF7* is required for optimal anti-tumor efficacy of human targeted T cells

(**A**) Graphs indicating expression of *IRF7, ISG15 and IFNB1* before (unstimulated) and after antigen activation (stimulated) detected by qPCR in sorted human T cells cotransduced with the 1928z CAR, 4-1BBL, a control shRNA ($1928z^+41BBL^+shK^+$) or an anti-*IRF7* shRNA ($1928z^+$ $41BBL^+$ $IRF7sh1^+$ and $1928z^+$ $41BBL^+$ $IRF7sh2^+$). Human T cells expressing $1928z^+LNGFR^+shK^+$ were included for comparison. Data are means ± SD. (**B**) Histograms showing IFNβ protein levels, measured by ELISA in cell lysates of indicated T cell groups expanded in vitro for 7 days and restimulated or not with irradiated NALM6 cells for 20 hr.

Data shown are representative of 5 independent experiments. Data are means ± SD. (**C**) IFNγ and granzyme B (GRZB) were detected by intracellular FACS staining 18 hr after antigen stimulation in indicated T cell groups from six different donors. Histograms show the average ± SEM of percentages of cells secreting the indicated molecules in CD4 or CD8 T cells. Values were normalized to that of $1928z^{+}41\text{-}BBL^{+}shK^{+}$ T cells in each donor to minimize inter-individual variability. (**D**) Impaired function induced by *IRF7* knockdown is rescued by addition of IFNβ. Intracellular cytokines were measured in the indicated T cell groups from four different donors, stimulated as in (**C**) in the absence or presence of IFNβ. Values were normalized to that of $1928z^{+}41BBL^{+}shK^{+}$ T cells in each donor to minimize inter-individual variability. Data are means ± SEM. (**E**) Plots representing the tumor burden weekly quantified by bioluminescence imaging per animal over a 50-day period. One line represents one mouse. n=4–6 mice per group. (**F**) Survival is illustrated in the Kaplan-Meier analysis. *p<0.05; **p<0.01; ***p<0.001. See also Figure S7.